https://doi.org/10.5194/egusphere-2026-4614
Preprint. Discussion started: 15 September 2026

Turbulent mixing at the polar jet and transport of cirrus particles into the lowermost extratropical stratosphere

Nicolas Emig [1], Annette K. Miltenberger [1], Heiko Bozem [1], Martina Krämer [1,†], Armin Afchine [2], Daniel Kunkel [1], Hans-Christoph Lachnitt [1], Yun Li [3], Philipp Reutter [1], Christian Rolf [2], Nicole Spelten [2], Holger Tost [1], and Peter M. Hoor [1]

[1]Institute for Atmospheric Physics, Johannes Gutenberg University Mainz, Mainz, Germany
[2]Institute of Climate and Energy Systems - Troposphere (ICE-4), Research Center Jülich, Jülich, Germany
[3]Institute of Climate and Energy Systems - Stratosphere (ICE-3), Research Center Jülich, Jülich, Germany
[†]formerly at 2

Correspondence: Nicolas Emig (niemig@uni-mainz.de)

Abstract.
The composition of the extratropical transition layer (ExTL), in particular the mixing ratios of ozone and water vapour, has a high impact on the radiative budget of the atmosphere. The ExTL is a transition region above the extratropical tropopause, characterized by smooth vertical gradients between typical tropospheric and stratospheric properties. It is shaped by several transport pathways, including quasi-isentropic mixing at the subtropical jet, diabatic descent from the stratosphere as part of the overturning circulation, and diabatic cross-tropopause exchange. The latter pathway is partially suppressed by the strong static stability above the tropopause, so that diabatic processes are necessary to facilitate mixing between the troposphere and the ExTL.

Here we present in situ measurements taken during the TPEx campaign in summer 2024 over the North Sea, that provide evidence for transport of ice particles through turbulent mixing across the tropopause caused by strong wind shears above the jet stream. The measurements are complemented by Lagrangian analyses of ICON model simulations for atmospheric context and history. High resolution acceleration measurements indicate turbulence while Lagrangian analysis shows suitable conditions for the turbulent mixing one hour prior to the measurements. Trace gas correlations and ice particle measurements confirm cross tropopause mixing through simultaneous occurrence of a stratospheric chemical signature and ice particles in subsaturation. With this combined analysis of measurements and simulations, we demonstrate that turbulent mixing is a potential pathway across the extratropical tropopause and that ice particles mixed into the stratosphere by this process possibly constitute a source of stratospheric water.

https://doi.org/10.5194/egusphere-2026-4614
Preprint. Discussion started: 15 September 2026

1 Introduction

The extratropical transition layer (ExTL, WMO (World Meteorological Organization), 2002) is a subregion of the upper troposphere–lower stratosphere (UTLS) that strongly modulates atmospheric composition and climate through exchange between the troposphere and the stratosphere (Riese et al., 2012; Hoor et al., 2002). It is characterized by vertical gradients of trace gas composition and a marked increase in static stability above the extratropical tropopause (Schäfler et al., 2021; Birner et al., 2002; Birner, 2006). Because ozone (O_3) and water vapour (H_2O) are radiatively active, even modest changes in their ExTL composition can introduce a disproportionate impact on radiative forcing and surface climate (Riese et al., 2012; Forster and Shine, 2002; Schäfler et al., 2021). While the troposphere is dominated by short transport and mixing time scales due to moist and dry diabatics, the stratosphere is a high-stability regime where vertical motion is strongly inhibited. The stratospheric composition therefore evolves on long time scales driven by the Brewer–Dobson circulation (BDC). The tropopause acts as a transport barrier marked by a sharp jump in static stability and by isentropic potential-vorticity (PV) gradients (Birner et al., 2002; Hoskins et al., 1985; Kunz et al., 2011). Two primary large-scale pathways control the ExTL composition. First: stratospheric downwelling (BDC) of ozone-rich, extremely dry air (4–7 ppmv H_2O, depending on season) which descends from the stratosphere, therefore reducing the water vapour mixing ratio in the ExTL (Butchart, 2014; Plumb, 2002; Tinney and Randel, 2026). Second: quasi-isentropic exchange across the subtropical jet is thought to be the dominant TST (Troposphere-to-Stratosphere Transport (Stohl et al., 2003)) mechanism, although additional pathways (e.g., deep convection, gravity-wave-driven exchange) also contribute. TST leads to air masses crossing the extratropical tropopause via diabatic processes and typically brings higher water vapour but lower ozone into the ExTL (Ray et al., 1999; Riese et al., 2012; Schäfler et al., 2021). Baroclinic wave activity shapes jet-stream position and strongly influences stratosphere-troposphere exchange. Tropopause folds and cut-off lows are associated with stratosphere-to-troposphere transport (STT Stohl et al. (2003)). Secondary circulations around jet streams contribute to this net transport (Shapiro, 1980). Jet streams are also a major source of vertical wind shear in the tropopause region, which can generate Kelvin-Helmholtz instabilities and turbulence (Shapiro, 1980; Kaluza et al., 2019; Spreitzer et al., 2019). Because turbulent mixing is effectively bidirectional and non-conservative, it can overcome tropopause stratification and promote exchange in both directions. Kunkel et al. (2019) documented in situ turbulence and mixing signatures in a baroclinic wave ridge, with the turbulent zone located just above the jet core on its anticyclonic flank. These processes which allow to overcome the transport barrier at the tropopause modify vertical tracer gradients in the stratosphere, with the barrier marked by a change of gradients from tropospheric to stratospheric conditions (Pan et al., 2004; Petzold et al., 2020; Lachnitt et al., 2023; Kunkel et al., 2016). Diabatic processes, which induce mixing and thus irreversible transport exhibit characteristic tracer–tracer correlations (e.g., N_2O–CO, N_2O–O_3) that are widely used to diagnose

https://doi.org/10.5194/egusphere-2026-4614
Preprint. Discussion started: 15 September 2026

irreversible stratosphere-troposphere exchange (STE) (Fischer et al., 2000; Hoor et al., 2002; Pan et al., 2004). However, such correlations are integrated diagnostics and, beyond case studies, cannot uniquely be assigned to the specific underlying physical processes or even time scales (Schäfler et al., 2021). The presence of upper-tropospheric cirrus clouds indicates diabatic activity (latent heat release, radiative cooling) and can provide a pathway for water-vapour and ice-particle transport across the tropopause. Climatologies of cirrus occurrence based on in situ measurements are discussed by Krämer et al. (2020), showing a general decrease in ice water content and particle sizes with altitude and accordingly very thin cirrus near the tropopause. Above the extratropical tropopause, usually at potential temperatures of Theta > 360K, the stratosphere becomes extremely dry (H_2O < 10 ppmv). Without local moisture sources by e.g. convective injections or cross tropopause mixing, stratospheric water vapour remains low and changes slowly. Due to increasing temperatures with altitude, relative humidity decreases for a fixed mixing ratio, and the stratosphere is typically subsaturated with respect to ice — a property recently used to define a tropopause metric (Reutter and Spichtinger, 2025). Under such conditions, ice particles are not expected to survive above the tropopause. However, remote-sensing observations have documented cirrus extending to or above the tropopause. Spang et al. (2002) detected thin cirrus around and above the tropopause using CRISTA infrared limb soundings. Pan and Munchak (2011) quantified 2–24% of cloud tops up to 2.5 km above the lapse-rate tropopause in tropical convection regions using CALIPSO and GFS reanalysis. Cirrus-related radiative processes have been investigated by Müürsepp et al. (2026) using Lagrangian methods and have been found to contribute substantially to troposphere-to-stratosphere transport. In the extratropical lowermost stratosphere, Müller et al. (2015) and Emig et al. (2025) showed that radiative cooling at the top of an existing cirrus layer can maintain saturation and sustain persistent cirrus above the tropopause. Overshooting convection can locally overcome the tropopause stability and irreversibly transport water vapour and ice particles (Mullendore et al., 2005; Konjari et al., 2025).

In this study we show an additional transport pathway of ice particles into the ExTL. We found evidence that shear-induced turbulence at the northern edge of the polar jet stream can transport ice particles across the extratropical tropopause. We base our analysis on in situ measurements from flight 10 (F10) on 20.06.2024 of the TPEx (TropoPause composition gradients and mixing Experiment) aircraft campaign in summer 2024 over the North Sea. We use measurements of N_2O, CO, O_3, H_2O, and ice particles to confirm cross-tropopause mixing, with special emphasis on the simultaneous occurrence of a stratospheric chemical signature and ice particles in a subsaturated air mass. The measurements are complemented by Lagrangian analyses of ICON (Icosahedral Nonhydrostatic) model simulations, which provide atmospheric context and the transport history of the sampled air masses. To identify turbulence as the responsible process, we use high-resolution acceleration measurements from a second platform that agree well with the occurrence and strength of simulated turbulence in ICON. The Lagrangian analysis indicates conditions favorable for turbulent mixing of cirrus particles about one hour before the measurements.

https://doi.org/10.5194/egusphere-2026-4614
Preprint. Discussion started: 15 September 2026

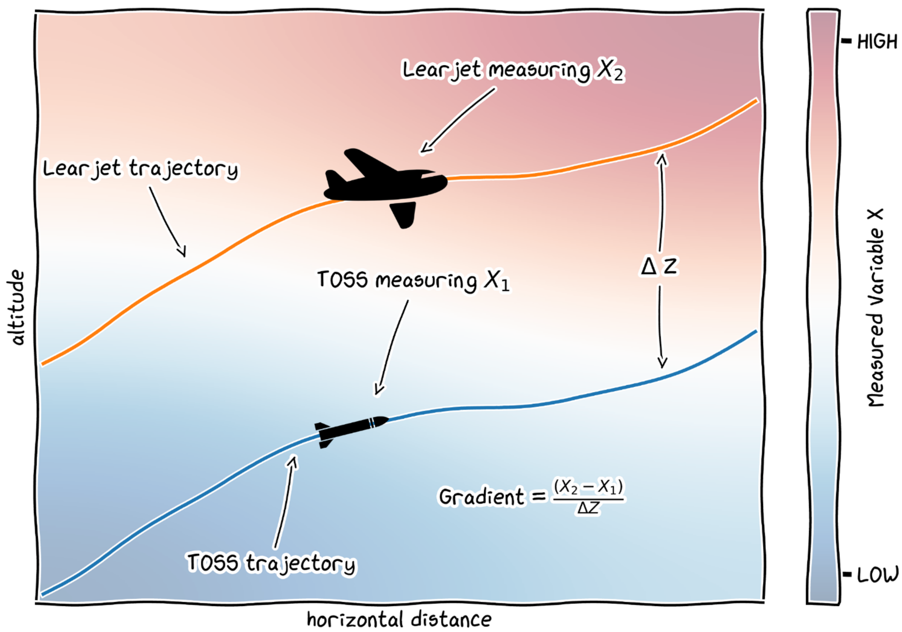

Figure 1. Schematic representation of the dual-platform-approach for the simultaneous measurement at two levels and calculation of vertical gradients. Background colours represent an arbitrary air mass property changing from low to high values at the tropopause, which can be measured simultaneously by the two platforms. Figure taken from Emig et al. (2025)

The paper is structured as follows: Section 2 describes the methods, Section 3 presents flight F10 and the synoptic situation, Section 4 analyzes air-mass composition to identify mixing, Section 5 discusses turbulence as the underlying process, and Section 6 concludes the study and outlines implications for stratospheric water budgets.

2 Methods

2.1 In situ Measurements:

The measurements discussed in this case study were taken during the TPEx (**T**ropo**P**ause compositon gradients and mixing **Ex**periment) aircraft campaign 2024 over Northern Germany. Main goal of the campaign was the investigation of the extratropical UTLS region and exchange processes. To this end, the aircraft, a Learjet type 35A, was equipped with instrumentation for in situ measurements of trace gases, aerosols and particles as well as meteorological parameters. As a special feature, a second platform towed by the Learjet with partially redundant instrumentation could be used to derive the vertical distribution of the mea-

https://doi.org/10.5194/egusphere-2026-4614
Preprint. Discussion started: 15 September 2026

sured quantities. This platform (the TropoPause Composition TOwed Sensor Shuttle, short TPC-TOSS) is described in detail in Bozem et al. (2025) and the measurement setup is illustrated in Fig. 1.

N_2O and CO mixing ratios were taken by the UMAQS (University Mainz airborne QCL Spectrometer) instrument on board the Learjet. UMAQS is an absorption spectrometer: A tunable quantum cascade diode laser emits a small section of the infrared spectrum, encompassing absorption lines of N_2O and CO. The radiation is partially absorbed in a Herriott-type multipass cell with an effective path length of 76 m and an actively controlled pressure of 53 hPa. From the transmission spectrum, the mixing ratios of N_2O and CO are calculated. UMAQS is calibrated in-flight with two different secondary standards of N_2O and CO. Spectral effects of water vapour and dilution are adjusted in post processing with information from the FISH instrument to achieve dry mixing ratios. The setup yields measurements with a frequency of 1 Hz and a total uncertainty of 0.39 ppbv in N_2O and 1.40 ppbv in CO, respectively (Müller et al., 2015).

O_3 mixing ratios were measured by TOMi (2BTech Ozone Monitor I) at the wingpod of the Learjet and TOMii (2BTech Ozone Monitor II) at the TPC-TOSS. TOMi and TOMii are "2BTech Model 205 dual beam ozone monitor" instruments utilizing UV absorption at a wavelength of 254 nm at ambient pressure. Both instruments were insulated and modified for operation in the Learjet wingpod and TPC-TOSS, respectively. The measurements of TOMi and TOMii have a time resolution of 0.5 Hz and a total uncertainty of 3 ppbv + 0.9 % for the TPC-TOSS and 3 ppbv + 0.7 % for the Learjet instrument (Bozem et al., 2025).

Static temperature and relative humidity were measured by two ICH (IAGOS capacitive hygrometer) sensors at the Learjet and the TPC-TOSS respectively. The ICH consists of a platinum resistance sensor (Pt100) that measures temperature and a thin-film capacitive sensor that measures the relative humidity. The ICH was developed for autonomous operation on passenger aircraft and is currently used within the framework of IAGOS (In-service Aircraft for a Global Observing System). A detailed description of the sensor can be found in Helten et al. (1998). For the TPEx campaign, the sensor has been calibrated before and after the campaign and after post-processing a remaining uncertainty of $\pm$0.32 K for the temperature and $\pm$ (5–6) % for the relative humidity is estimated following the quality assurance assessment of the sensors described in Neis et al. (2015) and references therein. The response time of the capacitive hygrometer depends strongly on the temperature, reaching orders of minutes for the coldest temperatures during F10. To achieve higher time resolution, we chose to calculate the relative humidities at Learjet level using the faster measurements of water vapour from the FISH instrument.

Ice particle measurements were taken by the NIXE-CAPS (New Ice eXpEriment – Cloud and Aerosol Particle Spectrometer (Luebke et al., 2016; Costa et al., 2017; Afchine et al., 2018)) instrument, which is a combination of CAS (Cloud and Aerosol Spectrometer) and a CIPg (Cloud Imaging Probe – grayscale). In combination, particles with diameters between 0.61 and 937 μm can be sized and counted. For cloud measurements, particle diameters > 3 μm are considered. This threshold is used as cloudindex.

Water vapour mixing ratios were measured by the FISH (Fast In situ Stratospheric Hygrometer) instrument.

https://doi.org/10.5194/egusphere-2026-4614
Preprint. Discussion started: 15 September 2026

The FISH provides high precision water vapour measurements by means of the Lyman-α photofragment fluorescence technique aboard research aircraft for almost 30 years (Zöger et al., 1999; Meyer et al., 2015). Based on the regular calibrations during the TPEx campaign, the overall accuracy of water vapour measurements with FISH is 4.9% or at least 0.77 ppmv. During F10, the inlet of the FISH pointed forwards in flight direction, capturing not only gas phase water vapour, but also evaporated ice particles in the presence of cirrus clouds. The measured water mixing ratios therefore represent the sum of all phases (= total water). To derive the gas phase water mixing ratios inside of cirrus, the ice water content measured by the NIXE-CAPS was substracted from the total water in post processing.

Two identical GNSS-aided inertial navigation systems of the type Microstrain 3DM-GQ7-GNSS/INS with two GNSS receiver antennas respectively were installed in the Learjet cabin and the TPC-TOSS. The geometric position for both platforms is provided with an uncertainty of 2 m in the vertical and 1.5 m in the horizontal direction and was logged with 1 Hz frequency. Acceleration measurements are available linearly in three spatial directions and angularly in three angles with a time resolution of 100 Hz and with a noise density of 20 μg/$\sqrt{}$Hz.

2.2 Derived quantities:

The static pressure at TPC-TOSS-level was calculated under the assumption of hydrostatic equilibrium from the pressure at Learjet level, the vertical distance between the two platforms as recorded by the GNSS devices, and the mean temperature between the two platforms, taken from the temperature measurements of the ICH sensors.

Relative humidity with respect to ice at the Learjet position was calculated using the water vapour mixing ratios captured by the FISH instrument. For the calculation of the partial pressure of water vapour, the pressure measurements from the Learjet were used. The relative humidity with respect to ice then only depends on the temperature, which was taken from the ICH sensor.

For lack of vertical wind measurements, we chose the 100 Hz z-acceleration measured by the 3DM-GQ7 devices to construct a proxy variable, since its behaviour is mainly dependent on the vertical wind on small time scales. As a qualitative approximation of the turbulent kinetic energy (TKE) we built a proxy variable implemented as the rolling variability of the mean standard deviation of the z-acceleration. For an idealized isotropic case this proxy would be proportional to the traditional TKE definition in one dimension. Since the z-acceleration does not depend only on the relative wind speeds but is also controlled by the connection to the Learjet, this approach fails for large time scales, but yields surprisingly sound results for short, potentially turbulent sections of the flight.

The same approximation was applied to calculate power spectra using the Welch-method (Welch, 1967). Additionally, a supposedly laminar section of the flight with low variability in z-acceleration was used to calculate a reference spectrum. The adjusted spectra (differences to the reference spectrum in log-space)

https://doi.org/10.5194/egusphere-2026-4614
Preprint. Discussion started: 15 September 2026

show the relative increase in activity with respect to the reference. The higher frequencies are dominated by the noise of the sensor.

2.3 Trajectory data

As complement to the in situ measurements and for detailed synoptic context regarding water vapour distribution, cloud formation, and flow, data from the operational ICON model (Zängl et al., 2015) analysis and short-term forecasts from German Weather Service (DWD) have been used. In particular, three-dimensional data was used from the European nest (ICON-EU), which covers the extended European domain with a horizontal grid spacing of 6.5 km. The ICON data was retrieved from the opendata.dwd.de during the campaign and is archived locally at JGU. To obtain an as accurate as possible representation of the atmosphere at a suitably high temporal resolution, we combined the 3-hourly analysis data with the short-term forecasts at 1 h and 2 h leadtime. Hence an estimate of the 3D state of the atmosphere is available at hourly resolution. Using the above ICON-EU data regridded onto a longitude-latitude grid air mass trajectories have been computed backward from the position of the Learjet as recorded by the GNNS receiver. The air mass trajectories were calculated using LAGRANTO (Sprenger and Wernli, 2015) adapted to ICON output data. Water vapour, hydrometeor mass mixing ratios, turbulent kinetic energy and other variables have been interpolated from the Eulerian grid to the trajectory position.

3 TPEx F10 - case description and synoptic situation

The case presented here is part of the last research flight of the TPEx campaign (F10) where evidence for strong mixing events associated with turbulence was encountered. The flight took place over the North Sea on June 20th 2024 between 07:00 and 10:00 UTC. The synoptic weather situation is depicted in Fig. 2. There was a ridge over Central and Eastern Europe (marked by the light yellow lines, showing the geopotential height in 500 hPa), slowly moving northwards, whose northern edge (and thus the jet stream) roughly followed the North Sea coast. In combination with a (cut-off) low over western Europe to the Iberian peninsula this produced a pronounced westerly to southwesterly flow at the measurement area with air masses originating as far south as Gibraltar, transporting considerable amounts of humidity. Fig. 2 also displays the satellite picture from the SEVIRI instrument in the visible channel at 7:00 UTC, i.e., the reflected shortwave radiation, indicating the cloud bands. Furthermore, the dashed magenta lines depict the surface pressure, with a high pressure ridge over Germany and mostly weak surface pressure gradients and a warm front located over Central Germany south of the flight area. However, equivalent potential temperature gradients (colour coded with opacity) were relatively weak over Europe, indicating only minor baroclinicity. The large-scale cloud field over France and Germany is associated with substantial lifting. However, this region was separated from the near-jet cirrus cloud, on which the measurements were concentrated. Fig. 3

https://doi.org/10.5194/egusphere-2026-4614
Preprint. Discussion started: 15 September 2026

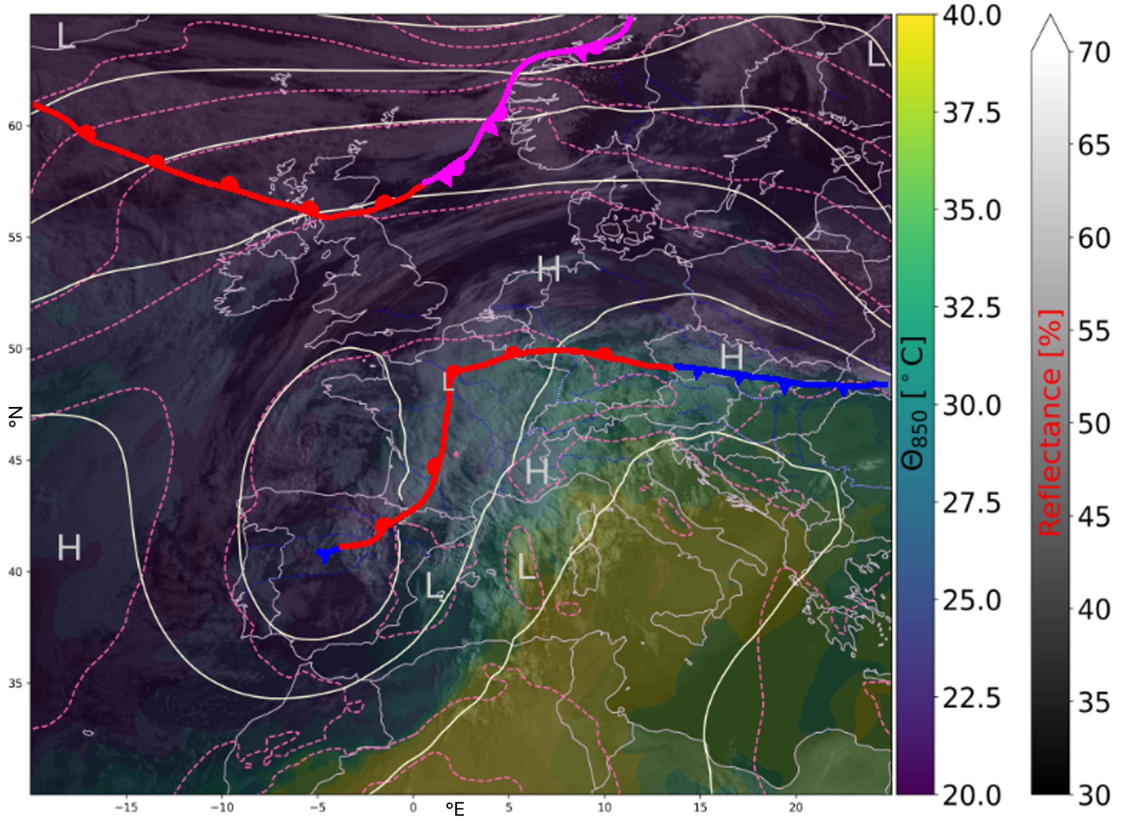

Figure 2. Synoptic situation for the 20th June 2024 over Europe at 7:00 UTC. The grey colour scale depicts the Meteosat SEVIRI (Spinning Enhanced Visible and Infrared Imager, MSG) visible satellite picture, the colour scale the equivalent potential temperature at 850 hPa. The thin light yellow lines mark the 500 hPa geopotential height and the dashed magenta lines the surface pressure. Frontal zones are manually included according to the analysis map of the German Weather Service for that specific time.

shows the flight track at the northern edge of the jet stream co-located with increased vertical shear of the horizontal wind as analyzed by ICON simulations. At time of measurement, the jet core was located at an altitude of roughly 10.5 km over the measurement area, with the flight track crossing its northern flank multiple times as depicted in Fig. 4. The blue and turquoise marks in the figure show in situ measurements of ice cloud particles consistent with the MSG satellite images in Fig. 2 and 3 with the turquoise marks indicating simultaneous occurrence of a chemically stratospheric signature in the trace gas measurements.

https://doi.org/10.5194/egusphere-2026-4614
Preprint. Discussion started: 15 September 2026

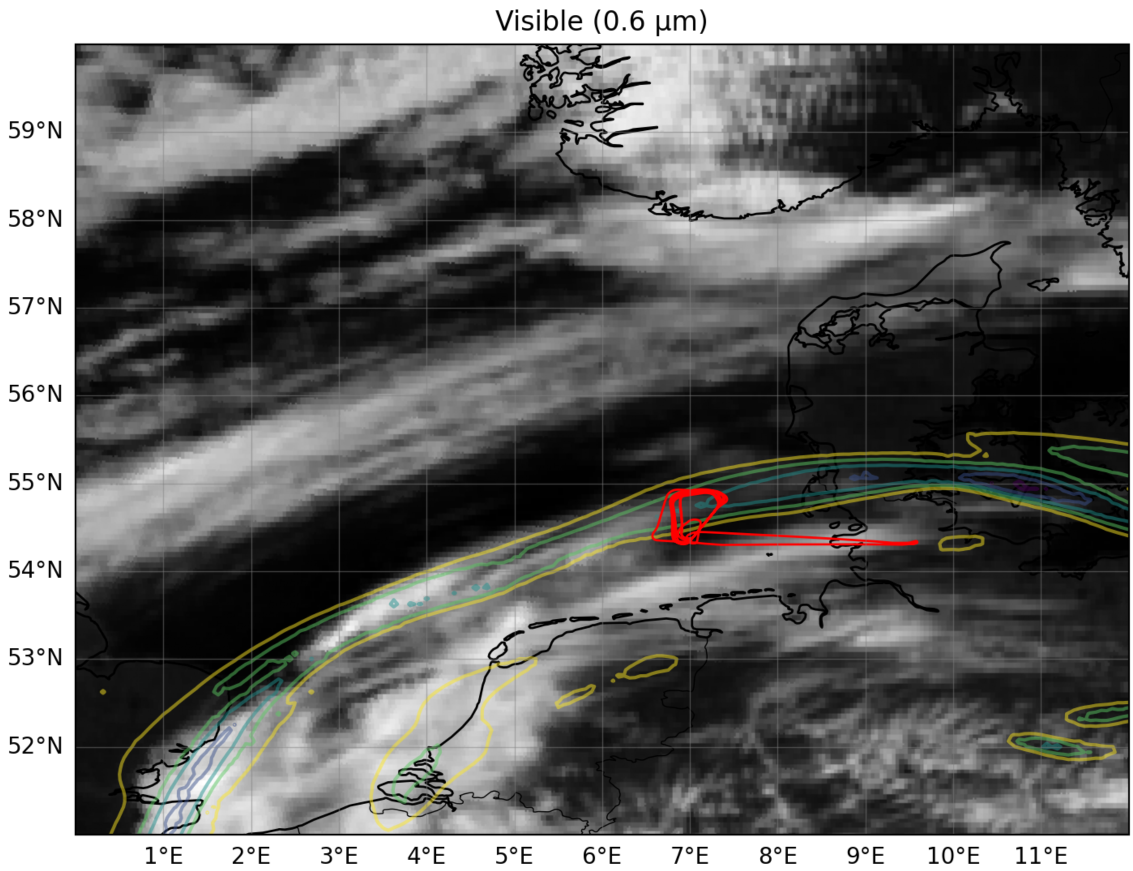

Figure 3. MSG satellite image (visible). F10 flight path marked in red. Contours show vertical shear of horizontal wind on the 250 hPa isosurface for June 20th 2024 09:00 UTC from ICON simulation.

4 Ice cloud particles and cross tropopause mixing

The flight path consisted of seven stacked levels in altitudes between 9000 and 11000 m. Ice particles were detected by the NIXE-CAPS instrument in the southern parts of the flightpath. The properties of the ice particles (see time series of particle size distributions in Fig. 5 (bottom), bottom panel) vary considerably throughout the flight, from high number concentrations and a broad distribution of sizes at FL 320 (around 9:15 UTC) to very thin cirrus with low number concentrations and a narrow distribution at FL 350 (around 8:45 UTC), which we will be the focus in this analysis. Note, that the relative humidity at flight level 350 is at 80% at maximum on this particular level and that the ice particles are found in subsaturated air (Fig. 5 (top)). At the highest level (FL 360, around 9:00 UTC), only two single particle events are detected. The position of the ice cloud relative to the flight path according to the ICON simulation is depicted in A1.

https://doi.org/10.5194/egusphere-2026-4614
Preprint. Discussion started: 15 September 2026

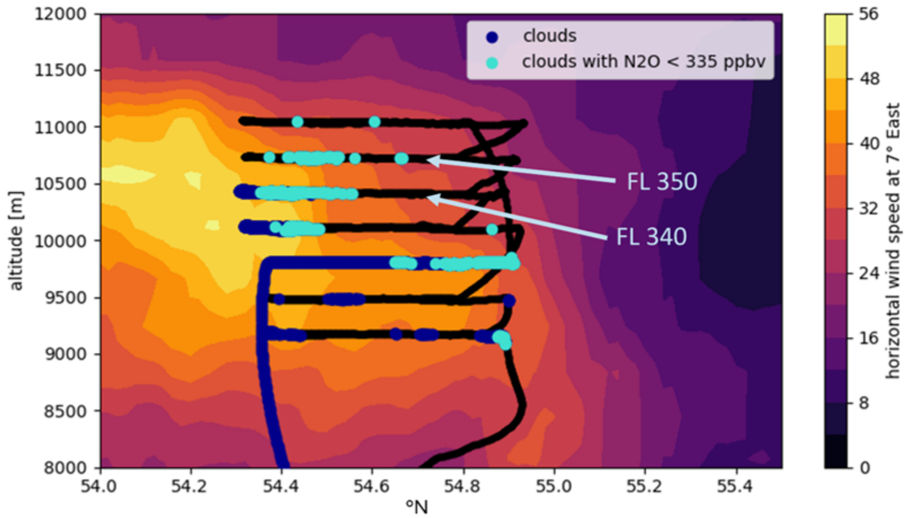

Figure 4. Geometric flight path of F10 (latitude vs altitude, black), horizontal wind speed for 08:00 from ICON simulation at 7°E in m/s as background shading. The measurements of cirrus particles are coloured in blue for tropospheric mixing ratios of nitrous oxide (N_2O > 335 ppbv) and turquoise for stratospheric mixing ratios (N_2O < 335 ppbv)

The mixing ratios of N_2O and CO show a similar behaviour characteristic for the ExTL. These tracers exhibit vertical gradients at the tropopause, as both have sources in the troposphere and sinks in the stratosphere. The tropospheric life time of N_2O is about 110 years (SPARC, 2012) which is long enough to consider the troposphere as well mixed (i.e. constant mixing ratios), particularly in the upper troposphere far from sources. Due to the stratospheric photolytic sink mixing ratios decrease with altitude leading to negative vertical gradients in the stratosphere.

This has two important implications for the analysis of exchange processes:

First, mixing ratios, especially of N_2O, that are lower than the tropospheric well mixed background, indicate an influence of stratospheric air at some point in the history of the respective air mass. We used this to construct a stratospheric marker in accordance with the method described in (Müller et al., 2015; Emig et al., 2025). Since the tropospheric mixing ratios of N_2O show a positive long term trend of >1 ppbv/year (NOAA, 2025), the respective tropospheric N_2O-values have to be adjusted, following the tropospheric trend. In this study, we use a conservative threshold of 335 ppbv, which is slightly lower than the mean tropospheric values for this campaign (around 336.9 ppbv) and therefore reduces false positives in the identification of chemically stratospheric air. Note, that the entire FL350 has mixing ratios of N_2O well below this threshold and is considered as stratospheric as highlighted in Fig. 6 (b). This is in good agreement with the model data, since the ICON simulations place this flight leg above the 2 PVU isosurface (see Fig. 7).

The second implication is that mixing events between the stratosphere with low N_2O and CO and the tropo-

https://doi.org/10.5194/egusphere-2026-4614
Preprint. Discussion started: 15 September 2026

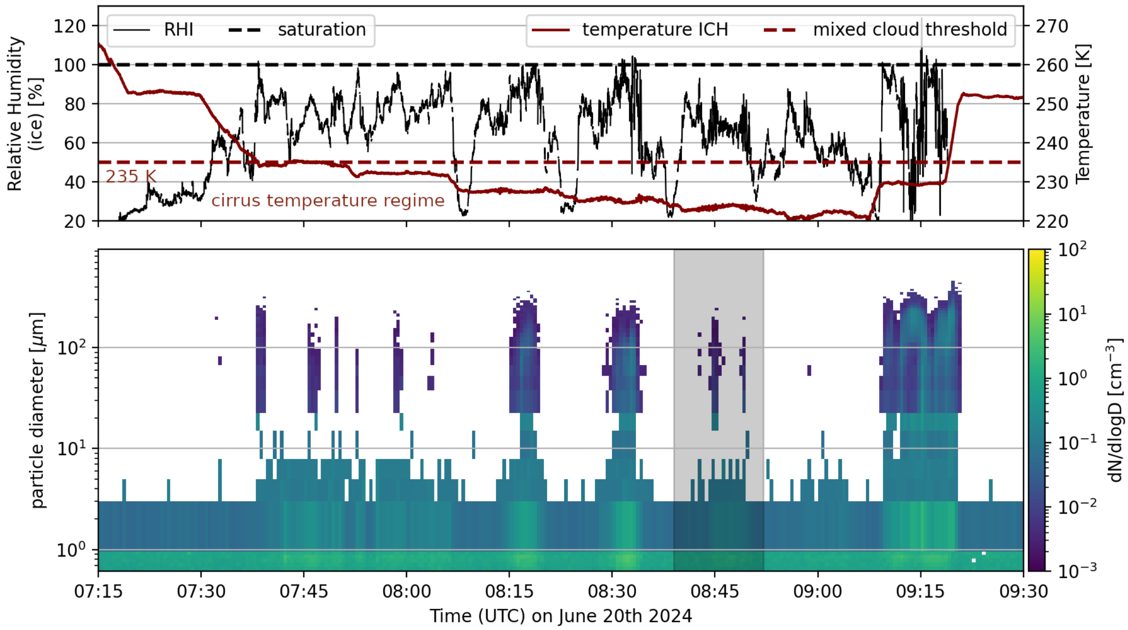

Figure 5. Time series of: (top) relative humidity with respect to (black) ice and air temperature (red; the dashed line (235 K) indicates the temperature below which only cirrus clouds prevail); (bottom) particle size distribution from the NIXE-CAPS instrument (particles > 3 µm are ice crystals; colour code is particle concentration). FL350 marked in gray box.

sphere with high mixing ratios of these tracers affect both species equally and produce intermediate states located on a "mixing line" in the tracer-tracer space. A compact correlation of spatially close measurement points therefore provides evidence for mixing. The corresponding correlation for this flight is shown in Fig 6.

The distribution of water vapour shows a similar distribution with very low values in the stratosphere, due to the low stratospheric values (controlled by tropical tropopause temperature), and variable but higher values in the troposphere. Accordingly, the relative humidity drops at the tropopause, which is reproduced in the model simulations (see Fig. 7) and reflected in our measurements: As expected, the lower the mixing ratios of N_2O and CO, the lower the relative humidity (see Fig. 6 (a)). Note, that N_2O mixing ratios decreasing below 335 ppbv clearly indicate stratospheric air. This correlation holds true if we select for datapoints with simultaneous measurements of cirrus particles, with a surprising fraction existing in subsaturated conditions, some of them down to 60% RH_i (see Fig. 6 (c)). This indicates that the cirrus particles have been encountered in stratospheric surrounding and were probably involved in a cross tropopause mixing process since in situ formation is not possible under the local subsaturated conditions. Furthermore, since the life time of these ice particles in the order of a few hours is short compared the life time of the chemical tracers,

https://doi.org/10.5194/egusphere-2026-4614
Preprint. Discussion started: 15 September 2026

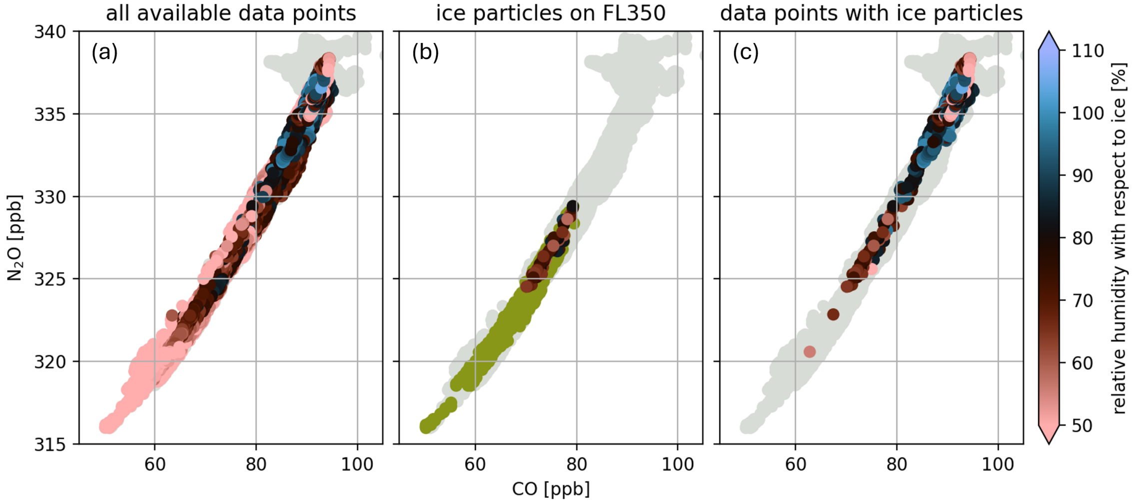

Figure 6. N_2O - CO correlations in tracer-tracer space, coloured by RH_i. Left: All data points where water vapour mixing ratios were available and relative humidity (RH_i) could be calculated. Middle: flight level FL350 with ice particles on FL350 coloured by RH_i and with data points where no ice particles were measured marked in green. Right: All data points with simultaneous measurements of ice particles. Note that data with N_2O<335 ppbv can be regarded as stratospheric, indicating ice particles distant from the tropopause for RH_i = 60-90%.

especially under these subsaturated conditions, the mixing event evident in the correlation could not have taken place long before the measurements. In a way, these particles can be viewed as very short lived tropospheric tracers, whose occurrence set a constraint in the order of hours on the time scale of the mixing process.

Additionally, we found occurrence of N_2O values lower than 335 ppbv well below the dynamical tropopause diagnosed by the model simulation (see Fig. 7) pointing to bidirectional transport. The region around the jet represents a region of increased horizontal and vertical shear. Such regions are favorable for the occurrence of turbulence leading to increased diffusivity that potentially overcomes the transport barrier at the jet and adiabatic PV conservation. Exchange takes place both from the troposphere to the stratosphere, as evidenced by cirrus particles, and in the opposite direction, as can be seen from the low N_2O mixing ratios below the dynamical tropopause.

In summary, we found evidence for bidirectional cross tropopause transport and mixing at the northern edge of the polar jet stream potentially associated with turbulence in the shear zones at the jet. From a trace gas perspective, this air mass is in a mixed state between tropospheric and stratospheric conditions. Additionally, it contained evaporating ice particles in subsaturated air, which is evidence for a very recent mixing event in the time scale of hours.

https://doi.org/10.5194/egusphere-2026-4614
Preprint. Discussion started: 15 September 2026

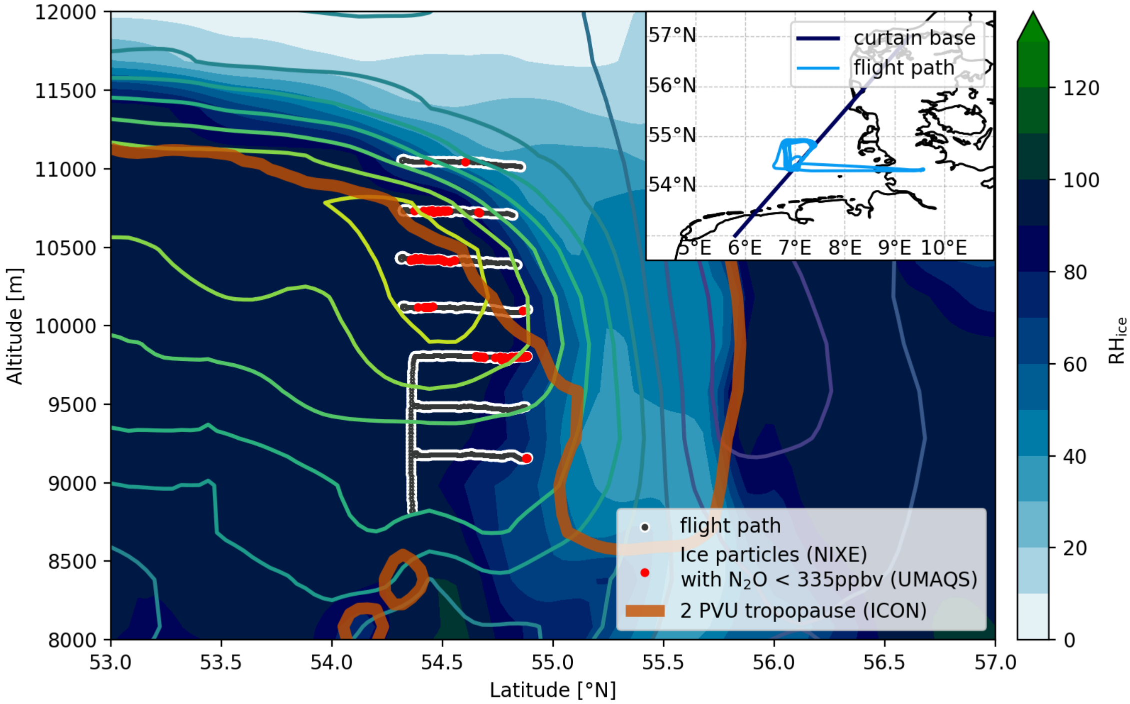

Figure 7. Cross section of the flight path of the Learjet during F10, cirrus particles with simultaneous measurements of N_2O < 335 ppbv marked in red. Relative humidity with respect to ice from ICON simulation as curtain. Contours of horizontal wind speed and 2 PVU-isosurface as tropopause. Top right: Map section of the North Sea with horizontal flight path (light blue) and curtain base (dark blue).

5 Turbulence as underlying process

To investigate the potential role of turbulence for the stratospheric ice particle abundance, we focus on FL350, which was entirely in the stratosphere from a chemical and dynamical perspective. The occurrence of ice particles at FL350 as shown by the teal dots in Fig. 8 (top) is most prominent on two sections at 08:45 and 08:49 UTC. At these sections we made several coinciding observations, each evidence for the occurrence of turbulence: As can be seen in Fig. 8 (top) the ice particles were encountered in regions of enhanced variability of N_2O. The mixing ratios are well below 335 ppbv indicating an entirely stratospheric environment. Notably the variability of the trace gas mixing ratios (also O_3 (Fig. 8 (middle) and CO (not shown)) prior and after the events is smaller, indicating that the variability is not noise driven but rather atmospheric.

Both findings are confirmed by the independent measurements of ozone on the Learjet and on the TPC-TOSS (Fig. 8 (middle)), showing values exceeding 160-360 ppbv, which is well above tropospheric values and showing enhanced variability during the events corresponding to N_2O-variability. Despite a vertical

https://doi.org/10.5194/egusphere-2026-4614
Preprint. Discussion started: 15 September 2026

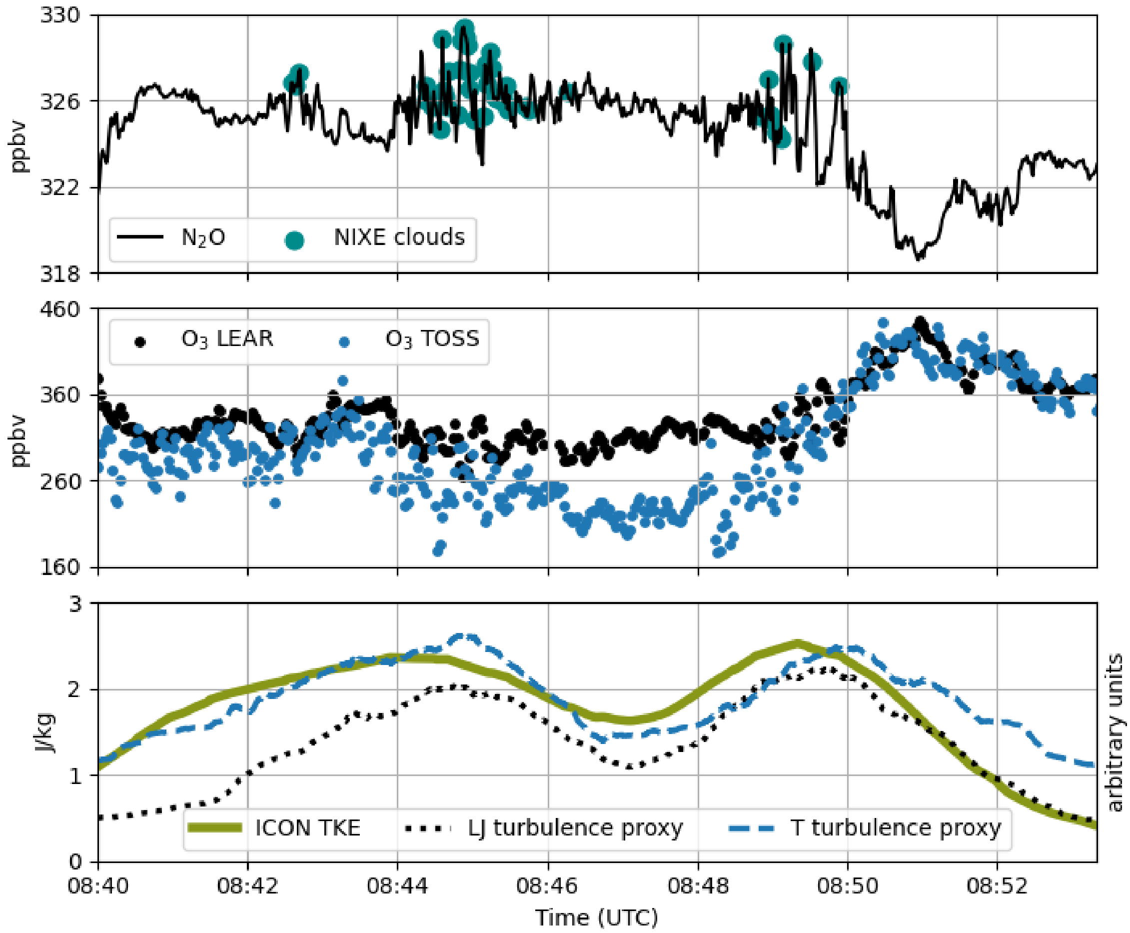

Figure 8. Time series of flight level 350 F10. N_2O mixing ratios in black, marked with NIXE-CAPS cloud index in teal to indicate cirrus occurrence (top). O_3 mixing ratios measured at the Learjet in black and at the TPC-TOSS in blue (mid). Turbulent kinetic energy from the ICON model simulation interpolated on the flight path in green, variability in z-acceleration measurements on the Learjet in black and on the TPC-TOSS in blue as turbulence proxy (bottom).

distance of around 150m between both platforms, the ozone measurements are relatively similar, indicating only a weak vertical gradient of ozone. This holds particularly for the regions with enhanced variability and is consistent with turbulent mixing, homogenizing vertical tracer gradients. Note that the regions before and after potential local turbulence also have very small differences in mixing ratios on both platforms at low variability, which could be remnants of earlier turbulent mixing before the measurements.

The increased variability in the atmospheric trace gases indicates the potential occurrence of turbulence, but it could also be explained by other phenomena such as gravity waves and therefore does not constitute direct evidence for currently ongoing mixing processes. Since we don't have access to accurate wind

https://doi.org/10.5194/egusphere-2026-4614
Preprint. Discussion started: 15 September 2026

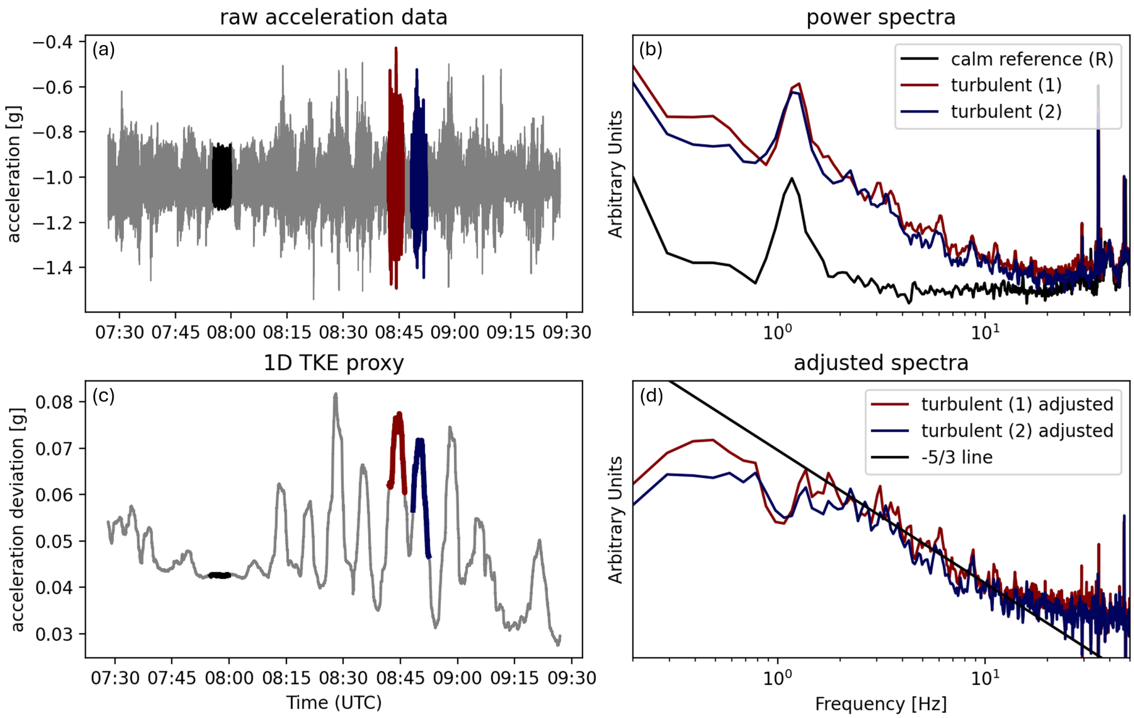

Figure 9. Time series of 100 Hz z-acceleration measurements for the entire time of TPC-TOSS operation for F10 (top left) with black highlight for the reference section, and red and blue for the (1) and (2) turbulent sections. Turbulence proxy (bottom left) with the same colour code as above. Raw power spectra (log-log, top right) and adjusted power spectra (log-log, bottom right) for the selected flight sections, coloured as above.

measurements for this campaign, in particular at the TPC-TOSS, the vertical acceleration (from now: z-acceleration) measurements were used to construct a proxy for turbulence occurrence. The z-acceleration of the TPC-TOSS on larger timescales is influenced by the cable connected to the Learjet. On smaller scales, however, it is directly affected by the vertical wind. Although the acceleration measurements do not allow for an absolute quantification of turbulence, the variability can be used as a proxy to determine the relative strength of the turbulent acceleration between flight segments. The variability z-acceleration shown in Fig. 8 (bottom) as rolling mean fits well to the model derived TKE from ICON. The structural agreement shows a good agreement between the measurements and the ICON simulation (see Fig. 8 (bottom)). The general behaviour is similar for the TPC-TOSS and the Learjet. The amplitude of the acceleration variations is more pronounced for the TPC-TOSS, most likely because the wind has a higher impact on the z-acceleration there, simply because it has less mass and inertia. Therefore, we will focus on the acceleration measurements on the TPC-TOSS only.

To test for a potential influence of turbulence on the acceleration measurements, we calculated power spec-

https://doi.org/10.5194/egusphere-2026-4614
Preprint. Discussion started: 15 September 2026

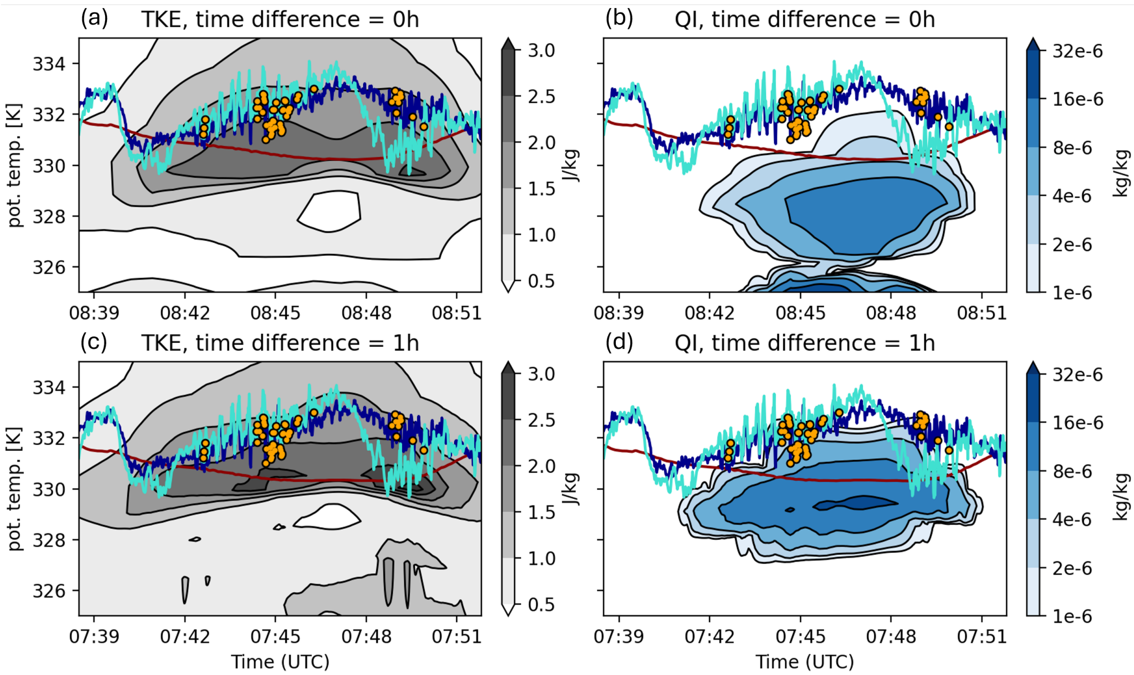

Figure 10. Curtains based on position of FL350 backward trajectories for turbulent kinetic energy (TKE, left) and cloud ice water content (Qi, right) of the ICON fields. Potential temperature as vertical coordinate on y-axis. Trajectory position at the respective time marked in red, potential temperature measurements from the Learjet (blue) and the TPC-TOSS (light blue). Detected cirrus particles marked in orange. The top row shows the curtains at time of flight, the bottom row one hour earlier.

tra using the Welch-method similar to Rodriguez Imazio et al. (2023). This method is a variant of the Fourier transform applied to overlapping segments of the time series, followed by averaging. In comparison with a Fourier transform of the continuous time series, the effects of random noise are reduced.

Fig. 9 shows acceleration data and power spectra for three different parts of the flight. Red and blue colours indicate the sections at FL350 where ice particles were encountered (at 08:45 UTC (1) and 08:49 UTC (2)). The section marked in black at around 07:55 in Fig. 9 (a) and (b) corresponds to measurements which were collected in quiet conditions and serves as reference (R). Several features visible in the spectra (1) and (2) in Fig. 9 (b) are present in each, the turbulent spectra (1) and (2) and the reference spectrum (R), and are therefore associated with the TPC-TOSS-cable-system itself rather than the atmospheric conditions: The pronounced peak at around 1 Hz with relatively high frequency-variance can be attributed to the flight behaviour of the TPC-TOSS, it is also present in the angular accelerations (not shown). Three sharper peaks at 48, 36 and 29 Hz are the 1/3, 1/4 and 1/5 resonance frequencies of 144 Hz and can be attributed to the vibrations of the pump of TOMii.

https://doi.org/10.5194/egusphere-2026-4614
Preprint. Discussion started: 15 September 2026

Relative to the reference spectrum, the spectra of the sections associated with enhanced tracer variability show an increased spectral density in all frequencies < 30 Hz (Fig. 9 (d)). The impact of turbulence on the z-acceleration of the TPC-TOSS acts on multiple scales, not just on discrete wavelengths, which would be the case for the influence of non-turbulent wavelike accelerations. Moreover, the comparison of the potentially turbulent and calm spectra resemble, at least partially, the -5/3 "Kolmogorov spectrum" characteristic for isotropic turbulence occurrence and the energy transfer from larger to smaller scales (Kolmogorov et al., 1991). It has to be noted, that this interpretation should be treated with caution, since the acceleration data does not quantitatively reflect the actual wind field.

At the measurement location both, local turbulence and cirrus particles are present. On the other hand ice particles, which were measured distant from the tropopause and which have been mixed prior to the measurements, already partly evaporated in subsaturated conditions. Having the good agreement of measured turbulence indication from the z-acceleration sensors and ICON along the flight track, we therefore used backward trajectories based on ICON simulations initialized at the flight path, to identify regions of high TKE at the tropopause. The enhancements of turbulent kinetic energy are co-located to the enhanced TKE at the time of measurements (t=0, Fig. 10 (a)), corresponding to the trajectories for the previously discussed sections of the flight path where ice particles were measured (Fig. 8 (top)) and the acceleration measurements indicated turbulence (Fig. 9). Following the backward trajectories in the ICON simulation, we found local maxima of TKE coinciding with the presence of ice water content around one hour before the measurements (see Fig. 10 (c) and (d)). Note that Fig. 10 uses potential temperature as vertical coordinate. The distribution of potential temperature relative to the flight path in geometric space is depicted in A2. One hour prior to the measurements the TKE along the backward trajectories was even larger consistent with the observed homogenization of the vertical gradient of ozone as evident in the small difference of ozone in Fig. 8 (middle).

Together, these findings suggest suitable conditions for the jet induced turbulent mixing of ice particles with dry air one hour prior to the measurements with subsequent transport and partial evaporation leading to the measured properties of the ice particles and observed air mass composition discussed above. Although the model simulation does not reproduce the conditions on the flight path perfectly, the features are remarkably consistent with the observations. Notably the temporal evolution confirms the hypotheses derived from the combined observational indications.

6 Conclusions

At the northern edge of the anticyclonic part of the polar jet stream, strong vertical shear of horizontal wind above the jet core caused turbulent mixing, transporting ice particles into subsaturated stratospheric air. This cross-tropopause mixing process was diagnosed directly in in situ measurements across several flight levels

https://doi.org/10.5194/egusphere-2026-4614
Preprint. Discussion started: 15 September 2026

above and below the tropopause, where ice occurrence above the tropopause is generally not expected. The short lifetime of these ice particles indicates the recency of the mixing event. Lagrangian analysis based on ICON model simulations reveals local maxima of turbulent kinetic energy coinciding with elevated cloud ice water content an hour prior to the observations, matching the position of the backward trajectories associated with in situ measurements of turbulence and stratospheric ice particles at time of flight. In summary, we captured the process and the immediate effect of turbulent mixing in in situ measurements, consistent with Lagrangian analysis of model simulations.

Another case of stratospheric cirrus particles was discussed by Emig et al. (2025), also using in situ trace gas measurements and Lagrangian methods. Emig et al. (2025) examine a slowly evolving warm front, with particles observed just above the tropopause (around 2 PVU) under supersaturated conditions. In that case, radiative cooling drives in situ ice formation from water vapour that was already present, implying that the cross-tropopause exchange of water vapour must have occurred several hours earlier. The study could show the dynamical impact of the cirrus itself due to the radiation driven diabatics leading to potential vorticity generation at cloud top. However the present study points out a completely different mechanism for the occurrence of cirrus in the stratosphere. Here we present strong evidence for jet-stream-induced turbulence as the driver of closely timed troposphere to stratosphere transport (TST). The ice particles were found in subsaturated conditions and ongoing mixing as indicated by the high range in N_2O values. Thus, cirrus particles can be regarded as a very short-lived tracer of the underlying exchange process into the stratosphere, being only sensitive for mixing within the timescale of existence of ice particles under subsaturated conditions which is on the order of hours. This time constraint adds important information compared to previous studies using long-lived species (e.g. N_2O, H_2O, CO) to diagnose STE (Schäfler et al., 2021; Hoor et al., 2004; Pan et al., 2004, e.g.).

The implication of this process is the transport of ice particles across the cold point due to frequent turbulent mixing at the jet, followed by evaporation, which could constitute an additional transport mechanism to convective overshoots of ice particles into the LMS (Konjari et al., 2025; Wang et al., 2011, e.g.) and contribute to a moistening of the lowermost stratosphere with an impact on the radiative budget.

However, in the context of this case study, the quantitative impact of this process on the water vapour content of the lower stratosphere remains unclear. Due to the limitations of both the spatial and temporal coverage of this single measurement flight the global relevance of this process must remain open. Statistical analyses based on ERA5 reanalysis data spanning 10 years by Kaluza et al. (2021) suggest that conditions for strong vertical wind shear near the tropopause in the ridges of baroclinic systems occur frequently. Kunkel et al. (2019) also discussed a similar synoptic situation involving turbulent mixing in a case study, backed up by idealized simulations. The situation described in the present study therefore does not appear to be synoptically unusual. However, the simultaneous presence of cirrus clouds in the region of shear driven turbulence has not yet been statistically investigated, which should be addressed in future research.

https://doi.org/10.5194/egusphere-2026-4614
Preprint. Discussion started: 15 September 2026

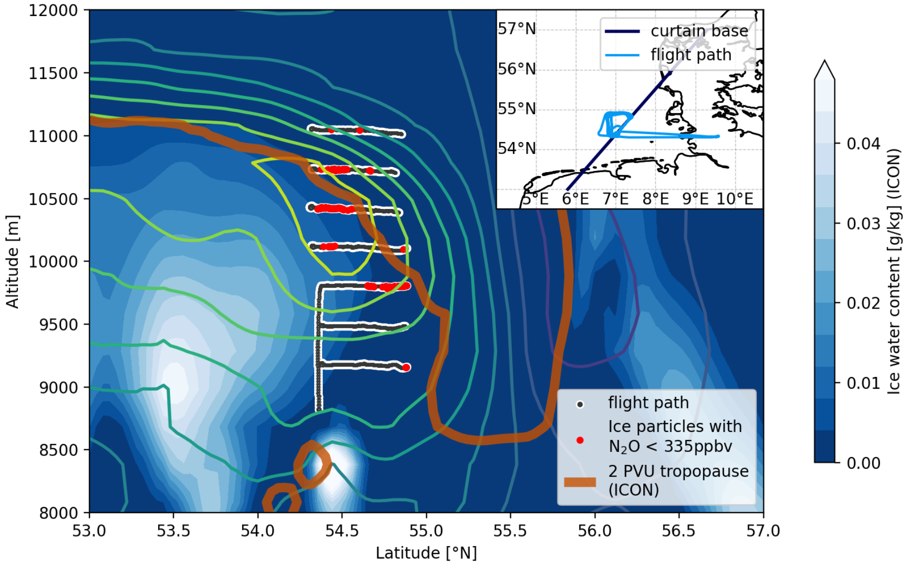

Figure A1. Cross section of the flight path of F10, cirrus particles with simultaneous measurements of N_2O < 335 ppbv marked in red. Cloud ice water content from ICON simulation as curtain. Contours of horizontal wind speed and 2 PVU-isosurface as tropopause. Top right: Map section of the North Sea with horizontal flight path and curtain base.

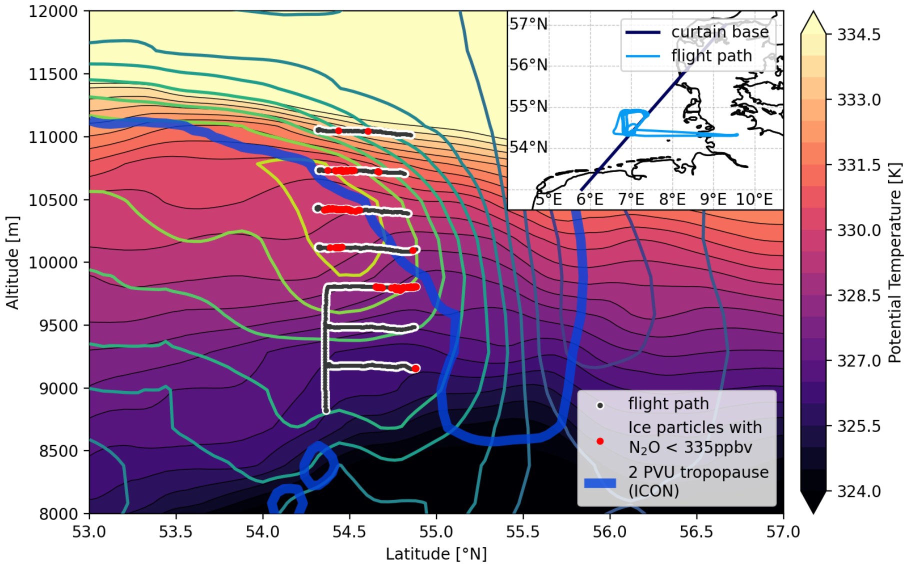

Figure A2. Cross section of the flight path of F10, cirrus particles with simultaneous measurements of N_2O < 335 ppbv marked in red. Potential temperature from ICON simulation as curtain. Contours of horizontal wind speed and 2 PVU-isosurface as tropopause. Top right: Map section of the North Sea with horizontal flight path and curtain base.

https://doi.org/10.5194/egusphere-2026-4614
Preprint. Discussion started: 15 September 2026

Code and data availability. The observational data and derived time series from the Learjet and TPC-TOSS, and and code for the creation of the figures will be published on Zenodo. The operational ICON data was retrieved from the opendata.dwd.de during the campaign and is archived locally at JGU. While the Eulerian data is available upon request from the authors, the trajectory data and the sub-set of the data to the flightpath will be published on Zenodo.

Author contributions. AM retrieved the operational data and conducted the calculations of the back trajectories; AA provided the ice particle data; NS provided the water vapour mixing ratio data; YL provided Temperature data; PR created the satellite image; HB and NE provided the N_2O and CO data and designed the TPC-TOSS; HCL compiled the merged data set; HT created the synoptic chart; PH designed the study and the TPEx-campaign; DK provided the forecast for the TPEx-campaign; All authors contributed to the writing of the manuscript.

Competing interests. At least one of the (co-)authors is a member of the editorial board of Atmospheric Chemistry and Physics.

Acknowledgements. The authors thank enviscope GmbH and GFD GmbH for enabling the TPEx campaign and the technical support. The authors acknowledge DWD, ECMWF and EUMETSAT for providing model data and satellite imagery. The authors thank Paola Imazio Rodriguez for useful input on the turbulence diagnostics.
The TPEx mission was funded by the Deutsche Forschungsgemeinschaft (DFG, German Research Foundation) – as part of the TRR 301 – Project-ID 428312742

https://doi.org/10.5194/egusphere-2026-4614
Preprint. Discussion started: 15 September 2026

References

Afchine, A., Rolf, C., Costa, A., Spelten, N., Riese, M., Buchholz, B., Ebert, V., Heller, R., Kaufmann, S., Minikin, A., Voigt, C., Zöger, M., Smith, J., Lawson, P., Lykov, A., Khaykin, S., and Krämer, M.: Ice particle sampling from aircraft – influence of the probing position on the ice water content, Atmospheric Measurement Techniques, 11, 4015–4031, https://doi.org/10.5194/amt-11-4015-2018, 2018.

Birner, T.: Fine-scale structure of the extratropical tropopause region, Journal of Geophysical Research Atmospheres, 111, D04 104, https://doi.org/10.1029/2005JD006301, 2006.

Birner, T., Dörnbrack, A., and Schumann, U.: How sharp is the tropopause at midlatitudes?, Geophysical Research Letters, 29, 45–1–45–4, https://doi.org/10.1029/2002GL015142, 2002.

Bozem, H., Joppe, P., Li, Y., Emig, N., Afchine, A., Breuninger, A., Curtius, J., Hofmann, S., Ismayil, S., Kandler, K., Kunkel, D., Kutschka, A., Lachnitt, H.-C., Petzold, A., Richter, S., Röschenthaler, T., Rolf, C., Schneider, L., Schneider, J., Vogel, A., and Hoor, P.: The TropoPause Composition TOwed Sensor Shuttle (TPC-TOSS): a new airborne dual platform approach for atmospheric composition measurements at the tropopause, Atmospheric Measurement Techniques, 18, 6545–6568, https://doi.org/10.5194/amt-18-6545-2025, 2025.

Butchart, N.: The Brewer-Dobson circulation, Reviews of Geophysics, 52, 157–184, https://doi.org/10.1002/2013RG000448, 2014.

Costa, A., Meyer, J., Afchine, A., Luebke, A., Günther, G., Dorsey, J. R., Gallagher, M. W., Ehrlich, A., Wendisch, M., Baumgardner, D., Wex, H., and Krämer, M.: Classification of Arctic, midlatitude and tropical clouds in the mixed-phase temperature regime, Atmospheric Chemistry and Physics, 17, 12 219–12 238, https://doi.org/10.5194/acp-17-12219-2017, 2017.

Emig, N., Miltenberger, A. K., Hoor, P. M., and Petzold, A.: Impact of cirrus on extratropical tropopause structure, Atmospheric Chemistry and Physics, 25, 13 077–13 101, https://doi.org/10.5194/acp-25-13077-2025, 2025.

Fischer, H., Wienhold, F. G., Hoor, P., Bujok, O., Schiller, C., Siegmund, P., Ambaum, M., Scheeren, H. A., and Lelieveld, J.: Tracer correlations in the northern high latitude lowermost stratosphere: Influence of cross-tropopause mass exchange, Geophysical Research Letters, 27, 97–100, 2000.

Forster, P. M. d. F. and Shine, K. P.: Assessing the climate impact of trends in stratospheric water vapor, Geophysical Research Letters, 29, 10–1–10–4, https://doi.org/10.1029/2001GL013909, 2002.

Helten, M. H. G. J. S., Sträter, W., Kley, D., Nedelec, P., Zöger, M., and Busen, R.: Calibration and performance of automatic compact instrumentation for the measurement of relative humidity from passenger aircraft, Journal of Geophysical Research: Atmospheres, 103, 25 643–25 652, https://doi.org/https://doi.org/10.1029/98JD00536, 1998.

Hoor, P., Fischer, H., Lange, L., Lelieveld, J., and Brunner, D.: Seasonal variations of a mixing layer in the lowermost stratosphere as identified by the CO-O3 correlation from in situ measurements, Journal of Geophysical Research: Atmospheres, 107, ACL 1–1–ACL 1–11, https://doi.org/10.1029/2000JD000289, 2002.

Hoor, P., Gurk, C., Brunner, D., Hegglin, M. I., Wernli, H., and Fischer, H.: Seasonality and extent of extratropical TST derived from in-situ CO measurements during SPURT, Atmospheric Chemistry and Physics, 4, 1427–1442, https://doi.org/10.5194/acp-4-1427-2004, 2004.

https://doi.org/10.5194/egusphere-2026-4614
Preprint. Discussion started: 15 September 2026

Hoskins, B. J., McIntyre, M. E., and Robertson, A. W.: On the use and significance of isentropic potential vorticity maps, Quarterly Journal of the Royal Meteorological Society, 111, 877–946, https://doi.org/10.1002/qj.49711147002, 1985.

Kaluza, T., Kunkel, D., and Hoor, P.: Composite analysis of the tropopause inversion layer in extratropical baroclinic waves, Atmospheric Chemistry and Physics, 19, 6621–6636, https://doi.org/10.5194/acp-19-6621-2019, 2019.

Kaluza, T., Kunkel, D., and Hoor, P.: On the occurrence of strong vertical wind shear in the tropopause region: a 10-year ERA5 northern hemispheric study, Weather and Climate Dynamics, 2, 631–651, https://doi.org/10.5194/wcd-2-631-2021, 2021.

Kolmogorov, A. N., Levin, V., Hunt, J. C. R., Phillips, O. M., and Williams, D.: The local structure of turbulence in incompressible viscous fluid for very large Reynolds numbers, Proceedings of the Royal Society of London. Series A: Mathematical and Physical Sciences, 434, 9–13, https://doi.org/10.1098/rspa.1991.0075, 1991.

Konjari, P., Rolf, C., Krämer, M., Afchine, A., Spelten, N., Bartolome Garcia, I., Miltenberger, A., Emig, N., Joppe, P., Schneider, J., Li, Y., Petzold, A., Bozem, H., and Hoor, P.: Stratospheric hydration and ice microphysics of a convective overshoot observed during the TPEx campaign over Sweden, Atmospheric Chemistry and Physics, 25, 18 031–18 050, https://doi.org/10.5194/acp-25-18031-2025, 2025.

Krämer, M., Rolf, C., Spelten, N., Afchine, A., Fahey, D., Jensen, E., Khaykin, S., Kuhn, T., Lawson, P., Lykov, A., Pan, L. L., Riese, M., Rollins, A., Stroh, F., Thornberry, T., Wolf, V., Woods, S., Spichtinger, P., Quaas, J., and Sourdeval, O.: A microphysics guide to cirrus – Part 2: Climatologies of clouds and humidity from observations, Atmospheric Chemistry and Physics, 20, 12 569–12 608, https://doi.org/10.5194/acp-20-12569-2020, 2020.

Kunkel, D., Hoor, P., and Wirth, V.: The tropopause inversion layer in baroclinic life-cycle experiments: the role of diabatic processes, Atmospheric Chemistry and Physics, 16, 541–560, https://doi.org/10.5194/acp-16-541-2016, 2016.

Kunkel, D., Hoor, P., Kaluza, T., Ungermann, J., Kluschat, B., Giez, A., Lachnitt, H. C., Kaufmann, M., and Riese, M.: Evidence of small-scale quasi-isentropic mixing in ridges of extratropical baroclinic waves, Atmos. Chem. Phys., 19, 12 607–12 630, https://doi.org/10.5194/acp-19-12607-2019, 2019.

Kunz, A., Konopka, P., Müller, R., and Pan, L. L.: Dynamical tropopause based on isentropic potential vorticity gradients, Journal of Geophysical Research, 116, D01 110, https://doi.org/10.1029/2010JD014343, 2011.

Lachnitt, H.-C., Hoor, P., Kunkel, D., Bramberger, M., Dörnbrack, A., Müller, S., Reutter, P., Giez, A., Kaluza, T., and Rapp, M.: Gravity-wave-induced cross-isentropic mixing: a DEEPWAVE case study, Atmospheric Chemistry and Physics, 23, 355–373, https://doi.org/10.5194/acp-23-355-2023, 2023.

Luebke, A. E., Afchine, A., Costa, A., Grooß, J.-U. U., Meyer, J., Rolf, C., Spelten, N., Avallone, L. M., Baumgardner, D., Krämer, M., M Avallone, L., Baumgardner, D., and Krämer, M.: The origin of midlatitude ice clouds and the resulting influence on their microphysical properties, Atmospheric Chemistry and Physics, 16, 5793–5809, https://doi.org/10.5194/acp-16-5793-2016, 2016.

Meyer, J., Rolf, C., Schiller, C., Rohs, S., Spelten, N., Afchine, A., Zöger, M., Sitnikov, N., Thornberry, T. D., Rollins, A. W., Bozóki, Z., Tátrai, D., Ebert, V., Kühnreich, B., Mackrodt, P., Möhler, O., Saathoff, H., Rosenlof, K. H., and Krämer, M.: Two decades of water vapor measurements with the FISH fluorescence hygrometer: a review, Atmospheric Chemistry and Physics, 15, 8521–8538, https://doi.org/10.5194/acp-15-8521-2015, 2015.

Mullendore, G. L., Durran, D. R., and Holton, J. R.: Cross-tropopause tracer transport in midlatitude convection, Journal of Geophysical Research D: Atmospheres, 110, 1–14, https://doi.org/10.1029/2004JD005059, 2005.

Müller, S., Hoor, P., Berkes, F., Bozem, H., Klingebiel, M., Reutter, P., Smit, H. G. J., Wendisch, M., Spichtinger, P., and Borrmann, S.: In situ detection of stratosphere-troposphere exchange of cirrus particles in the midlatitudes, Geophysical Research Letters, 42, 949–955, https://doi.org/10.1002/2014GL062556, 2015.

Müürsepp, T., Sprenger, M., Wernli, H., and Joos, H.: The role of radiation in the Northern Hemisphere troposphere-to-stratosphere transport, Weather and Climate Dynamics, 7, 547–565, https://doi.org/10.5194/wcd-7-547-2026, 2026.

Neis, P., Smit, H. G., Krämer, M., Spelten, N., and Petzold, A.: Evaluation of the MOZAIC Capacitive Hygrometer during the airborne field study CIRRUS-III, Atmospheric Measurement Techniques, 8, 1233–1243, https://doi.org/10.5194/amt-8-1233-2015, 2015.

Pan, L. L. and Munchak, L. A.: Relationship of cloud top to the tropopause and jet structure from CALIPSO data, Journal of Geophysical Research Atmospheres, 116, 1–17, https://doi.org/10.1029/2010JD015462, 2011.

Pan, L. L., Randel, W. J., Gary, B. L., Mahoney, M. J., and Hintsa, E. J.: Definitions and sharpness of the extratropical tropopause: A trace gas perspective, Journal of Geophysical Research D: Atmospheres, 109, 1–11, https://doi.org/10.1029/2004JD004982, 2004.

Petzold, A., Neis, P., Rütimann, M., Rohs, S., Berkes, F., Smit, H. G. J., Krämer, M., Spelten, N., Spichtinger, P., Nédélec, P., and Wahner, A.: Ice-supersaturated air masses in the northern mid-latitudes from regular in situ observations by passenger aircraft: vertical distribution, seasonality and tropospheric fingerprint, Atmospheric Chemistry and Physics, 20, 8157–8179, https://doi.org/10.5194/acp-20-8157-2020, 2020.

Plumb, R. A.: Stratospheric Transport., Journal of the Meteorological Society of Japan, 80, 793–809, https://doi.org/10.2151/jmsj.80.793, 2002.

Ray, E. A., Moore, F. L., Elkins, J. W., Dutton, G. S., Fahey, D. W., Vömel, H., Oltmans, S. J., and Rosenlof, K. H.: Transport into the northern hemisphere lowermost stratosphere revealed by in situ tracer measurements, Journal of Geophysical Research: Atmospheres, 104, 26 565–26 580, https://doi.org/https://doi.org/10.1029/1999JD900323, 1999.

Reutter, P. and Spichtinger, P.: The frosty frontier: redefining the mid-latitude tropopause using the relative humidity over ice, Atmospheric Chemistry and Physics, 25, 16 303–16 314, https://doi.org/10.5194/acp-25-16303-2025, 2025.

Riese, M., Ploeger, F., Rap, A., Vogel, B., Konopka, P., Dameris, M., and Forster, P.: Impact of uncertainties in atmospheric mixing on simulated UTLS composition and related radiative effects, Journal of Geophysical Research Atmospheres, 117, 1–10, https://doi.org/10.1029/2012JD017751, 2012.

Rodriguez Imazio, P., Mininni, P. D., Godoy, A., Rivaben, N., and Dörnbrack, A.: Not All Clear Air Turbulence Is Kolmogorov—The Fine-Scale Nature of Atmospheric Turbulence, Journal of Geophysical Research: Atmospheres, 128, e2022JD037 491, https://doi.org/10.1029/2022JD037491, e2022JD037491 2022JD037491, 2023.

Schäfler, A., Fix, A., and Wirth, M.: Mixing at the extratropical tropopause as characterized by collocated airborne H_2O and O_3 lidar observations, Atmospheric Chemistry and Physics, 21, 5217–5234, https://doi.org/10.5194/acp-21-5217-2021, 2021.

https://doi.org/10.5194/egusphere-2026-4614
Preprint. Discussion started: 15 September 2026

Shapiro, M. A.: Turbulent Mixing within Tropopause Folds as a Mechanism for the Exchange of Chemical Constituents between the Stratosphere and Troposphere, Journal of the Atmospheric Sciences, 37, 994–1004, https://doi.org/10.1175/1520-0469(1980)037<0994:TMWTFA>2.0.CO;2, 1980.

Spang, R., Eidmann, G., Riese, M., Offermann, D., Preusse, P., Pfister, L., and Wang, P.-H.: CRISTA observations of cirrus clouds around the tropopause, Journal of Geophysical Research: Atmospheres, 107, CRI 2–1–CRI 2–18, https://doi.org/https://doi.org/10.1029/2001JD000698, 2002.

Spreitzer, E., Attinger, R., Boettcher, M., Forbes, R., Wernli, H., and Joos, H.: Modification of potential vorticity near the tropopause by nonconservative processes in the ECMWF model, Journal of the Atmospheric Sciences, 76, 1709–1726, https://doi.org/10.1175/JAS-D-18-0295.1, 2019.

Sprenger, M. and Wernli, H.: The LAGRANTO Lagrangian analysis tool – version 2.0, Geoscientific Model Development, 8, 2569–2586, https://doi.org/10.5194/gmd-8-2569-2015, 2015.

Stohl, A., Bonasoni, P., Cristofanelli, P., Collins, W., Feichter, J., Frank, A., Forster, C., Gerasopoulos, E., Gäggeler, H., James, P., Kentarchos, T., Kromp-Kolb, H., Krüger, B., Land, C., Meloen, J., Papayannis, A., Priller, A., Seibert, P., Sprenger, M., Roelofs, G. J., Scheel, H. E., Schnabel, C., Siegmund, P., Tobler, L., Trickl, T., Wernli, H., Wirth, V., Zanis, P., and Zerefos, C.: Stratosphere-troposphere exchange: A review, and what we have learned from STACCATO, Journal of Geophysical Research: Atmospheres, 108, https://doi.org/10.1029/2002JD002490, 2003.

Tinney, E. N. and Randel, W. J.: Characterizing variability and vertical structure of water vapor in the extratropical lower stratosphere, EGUsphere, 2026, 1–25, https://doi.org/10.5194/egusphere-2026-412, 2026.

Wang, P. K., Su, S. H., Charvát, Z., Šťástka, J., and Lin, H. M.: Cross tropopause transport of water by mid-latitude deep convective storms: A review, Terrestrial Atmospheric Oceanic Sciences, 22, 447–462, https://doi.org/10.3319/TAO.2011.06.13.01(A), 2011.

Welch, P.: The use of fast Fourier transform for the estimation of power spectra: A method based on time averaging over short, modified periodograms, IEEE Transactions on Audio and Electroacoustics, 15, 70–73, https://doi.org/10.1109/TAU.1967.1161901, 1967.

WMO (World Meteorological Organization): Scientific Assessment of Ozone Depletion: 2002, in: WMO (World Meteorological Organization) Scientific Assessment of Ozone Depletion: 2002, Global Ozone Research and Monitoring Project - Report No. 47, 498pp., Geneva, 2003., World Meteorological Organization, Geneva, Switzerland, 2002.

Zängl, G., Reinert, D., Rípodas, P., and Baldauf, M.: The ICON (ICOsahedral Non-hydrostatic) modelling framework of DWD and MPI-M: Description of the non-hydrostatic dynamical core, Quarterly Journal of the Royal Meteorological Society, 141, 563–579, https://doi.org/10.1002/qj.2378, 2015.

Zöger, M., Afchine, A., Eicke, N., Gerhards, M.-T., Klein, E., McKenna, D. S., Mörschel, U., Schmidt, U., Tan, V., Tuitjer, F., Woyke, T., and Schiller, C.: Fast in situ stratospheric hygrometers: A new family of balloon-borne and airborne Lyman α photofragment fluorescence hygrometers, Journal of Geophysical Research: Atmospheres, 104, 1807–1816, https://doi.org/https://doi.org/10.1029/1998JD100025, 1999.